Semiclassical surfacehopping approximations for the calculation of solvent induced vibrationalrelaxation rate constants

Julio C. Arce and Michael F. Herman

Citation: J. Chem. Phys. **101**, 7520 (1994); doi: 10.1063/1.468245
View online: http://dx.doi.org/10.1063/1.468245
View Table of Contents: http://jcp.aip.org/resource/1/JCPSA6/v101/i9
Published by the American Institute of Physics.

Semiclassical surface-hopping approximations for the calculation of solvent-induced vibrational-relaxation rate constants

Julio C. Arce and Michael F. Herman
Department of Chemistry, Tulane University, New Orleans, Louisiana 70118

(Received 14 June 1994; accepted 22 July 1994)

Approximate schemes for the calculation of the rates of transitions between vibrational states of a molecule due to the interactions with a solvent are devised based on a rigorous, general semiclassical surface-hopping formalism developed earlier. The formal framework is based on an adiabatic separation of time scales between the fast molecular vibrations and the relatively slow bath motions. (The bath is composed of the solvent degrees of freedom plus all the molecular degrees of freedom other than vibrations.) As a result, the dynamics of the system are described in terms of bath motions occurring on adiabatic vibrational-energy surfaces, which are coupled by a nonadiabatic interaction. The time-dependent vibrational transition probability is evaluated by propagating the canonical density of the system, with the molecule in the initial adiabatic vibrational state, forward in time, and then projecting it onto the final adiabatic vibrational state of interest. The temporal evolution of the density is carried out with a semiclassical surface-hopping propagator, in which the motion of the bath on an adiabatic vibrational surface is described in terms of the familiar (adiabatic) semiclassical propagator, while transitions are accounted for in terms of instantaneous hops of the bath paths between the adiabatic vibrational surfaces involved, with an integration over all possible hopping points. Energy is conserved in the hops, and the only component of momentum that changes is the one along the nonadiabatic coupling vector. When the nonadiabatic interaction is taken into account to first order, the transition probability is predicted to become linear in the long-time limit. Various methods for extracting the relaxation rate constant in this limit are presented, and a simple model system with a one-dimensional bath is employed to compare their practical efficiency for finite time. In addition, this system is used to numerically demonstrate that local approximations for the adiabatic vibrational surfaces and the nonadiabatic coupling yield accurate results, with great reduction of the amount of computation time. Since a local approximation for the vibrational surfaces makes an N-dimensional problem separable into N effectively one-dimensional ones, this treatment is seen to be more generally applicable to realistic systems.

I. INTRODUCTION

In this article, we present several approximate schemes for the calculation of the rate constants of vibrational transitions induced in a molecule by the interactions with a solvent. These approximations stem from a rigorous formal framework recently developed,[1] which, in turn, employs a semiclassical surface-hopping propagator introduced earlier for the study of nonadiabatic processes in general.[2]

The formalism is based on an adiabatic separation of time scales between the fast molecular vibrational motions and the slow bath motions,[3] analogous to the familiar Born–Oppenheimer separation of the electronic and the relatively slow nuclear degrees of freedom.[4] (The bath is the collection of all the degrees of freedom of the system other than the molecular vibrations.) As a result, the dynamics of the system are described in terms of bath motions occurring on adiabatic vibrational-energy surfaces. Transitions between these surfaces are induced by a nonadiabatic interaction, which couples the vibrational and bath degrees of freedom.

The initial state of the entire system is represented by the canonical density of the joint molecule–bath system, projected onto the initial adiabatic vibrational state. (If desired, the density can be treated within the adiabatic approximation.) The vibrational transition probability is evaluated by propagating the initial density forward in time and then projecting it onto the final adiabatic vibrational state of interest.

This formal description of the process corresponds to the usual experimental interpretation, in which the solute molecules are pictured as being initially prepared in an "excited vibrational state" by, e.g., a laser pulse. The subsequent decay over time of the excited population, due to the interactions with the solvent, is monitored, whereas the state of the bath remains unobserved at all times.

The temporal propagation of the density matrix is carried out with the semiclassical surface-hopping propagator mentioned above, in which the motion of the bath coordinates on an adiabatic vibrational surface is described by means of the familiar semiclassical propagator,[5] whereas transitions are accounted for in terms of instantaneous hops of the bath paths between the adiabatic vibrational surfaces involved, with an integration over all possible hopping points.[2] The hops conserve energy and the only component of the momentum that changes is the one along the direction of the nonadiabatic coupling vector.

This approach is in the same spirit as the method recently developed by Tully for nonadiabatic problems.[6] The difference is that in Tully's method, trajectories hop between adiabatic surfaces according to a stochastic "fewest switches criterion," whereas in our theory, the time and location of the

 0021-9606/94/101(9)/7520/8/$6.00

hops, as well as the hopping amplitude, are governed by an analytical prescription. In practice, in our method, the integration over hopping points can be performed either analytically or numerically, depending on the application and the level of approximation.

When only the first-order contribution in the nonadiabatic coupling to the propagator is employed, a second-order expression for the time-dependent transition probability is obtained.[1] This expression predicts that, in the long-time limit, the second-order transition probability becomes linear with time, in accordance with Fermi's golden rule.[7] We present three ways in which the vibrational-relaxation rate constant can be extracted from this development. Although, formally, these approaches are equivalent, in practice, this is not necessarily the case. The comparison of the performance of these three methods for finite time is one of the objectives of this work. For our numerical tests, we employ a simple model system consisting of a bromine molecule enclosed between two fixed argon atoms.

It must be emphasized that, in this approach, the linear behavior of the time-dependent transition probability emerges naturally in the long-time regime. This is a consequence of the incoherent temporal evolution of the state of the molecule due to the interactions with the solvent. The need to look at the long-time behavior of the transition probability in order to extract the rate constant may appear to render this framework rather computationally demanding. However, this is not necessarily so if the long-time limit is achieved relatively quickly in practice. It will be shown that, indeed, this is the case for the model system studied here and that there is good reason to expect this to occur in realistic systems as well.

This situation is analogous to what happens in approaches that begin directly with the golden rule,[7] in which rate constants are obtained as Fourier transforms of suitably defined time correlation functions. Although, in principle, the Fourier transform implies an infinite record of time, such correlation functions usually decay rapidly, allowing the calculation to be performed successfully with a relatively small range of time.

An obvious advantage of our formal framework over golden-rule-based approaches[7] is that it allows the explicit evaluation of the entire temporal evolution of the transition probability, permitting the study of short-time phenomena, e.g., transient effects. Another advantage of this approach is that the nonadiabatic coupling can, in principle, be taken into account up to any desired order.

Moreover, since our framework is formally rigorous, it can serve as the basis for the development of approximations whose accuracy can be readily assessed. Here, we demonstrate that local approximations for the adiabatic vibrational surfaces and the nonadiabatic coupling yield good accuracy for the calculation of the rate constant. For realistic problems, these approximations should represent enormous computational savings.

For ease of reference, the basic aspects of the theory pertinent to this work are reviewed in Sec. II, including the different expressions from which the vibrational-relaxation rate constant can be obtained. In Sec. III, after describing the nature of our model system, we present numerical results that establish the validity and practicality of the formal expressions obtained in Sec. II, and of the local approximations for the adiabatic surfaces and the nonadiabatic coupling. We close with some concluding remarks in Sec. IV.

II. THEORY

The general formalism on which this work is based was developed in Ref. 1. Here, we only present a summary of that development. The system to which this theory applies consists of a molecule immersed in a gas or liquid at high temperature.[8]

Due to the molecule–solvent interaction, the total Hamiltonian is not separable into vibrational and bath parts, i.e., molecular vibrational states are not eigenstates of the entire system. In this work, we employ adiabatic vibrational states as a convenient definition. These states are solutions of the adiabatic vibrational Schrödinger equation

$$\hat{H}^{\nu}(\mathbf{r},\mathbf{R})\,\psi_{\kappa}^{\nu}(\mathbf{r},\mathbf{R})=E_{\kappa}^{\nu}(\mathbf{R})\,\psi_{\kappa}^{\nu}(\mathbf{r},\mathbf{R}). \tag{1}$$

Here, $\hat{H}^{\nu}(\mathbf{r},\mathbf{R})=\hat{T}^{\nu}+\hat{V}^{\nu}(\mathbf{r})+V_{\rm int}(\mathbf{r},\mathbf{R})$ is the adiabatic vibrational Hamiltonian operator, where $\hat{T}^{\nu}$ is the vibrational kinetic-energy operator, V^{ν} is the vibrational potential, and $V_{\rm int}$ is the molecule–solvent interaction potential; ψ_{κ}^{ν} and E_{κ}^{ν} are the κth adiabatic vibrational wave function and energy, respectively; and $\mathbf{r}$, $\mathbf{R}$ are the vibrational and bath coordinates, respectively. The total Hamiltonian is then written as $\hat{H}=\hat{H}^{\nu}+\hat{T}^{b}+V^{s}$, with $\hat{T}^{b}$ the bath kinetic-energy operator and V^{s} the solvent–solvent interaction potential. The adiabatic approximation amounts to neglecting the action of T^{b} on the ψ_{κ}^{ν}.

The probability of finding the molecule in the adiabatic vibrational state $|f\rangle$ at time t, if it was in the state $|i\rangle$ at $t=0$, is given by

$$P_{if}(t)=Q_{i}^{-1}\ \mathrm{Tr}\ K_{if}(t)\rho_{ii}K_{if}^{\dagger}(t). \tag{2a}$$

Here, Tr denotes the trace over the bath degrees of freedom; $K_{if}(t)\equiv\langle f|\hat{U}(t)|i\rangle$ is the transition matrix element of the propagator, where $\hat{U}(t)=\exp(-i\hat{H}t/\hbar)$ is the time-evolution operator, $\hat{H}$ being the Hamiltonian for the entire molecule–solvent system; $\rho_{ii}\equiv\langle i|\hat{\rho}|i\rangle$, where $\hat{\rho}=\exp(-\beta\hat{H})$ is the canonical-density operator, with $\beta\equiv1/(\kappa_B T)$; finally, $Q_i\equiv\mathrm{Tr}\,\rho_{ii}$ is the canonical partition function of the system when the molecule is in state $|i\rangle$. In the coordinate representation of the bath degrees of freedom, the transition probability can be expressed as

$$P_{if}(t)=Q_{i}^{-1}\int d\mathbf{R}_f\,\mathbf{R}_{ia}\,d\mathbf{R}_{ib}\,K_{if}(\mathbf{R}_{ia},\mathbf{R}_f,t)\times\rho_{ii}(\mathbf{R}_{ia},\mathbf{R}_{ib},\beta)K_{if}^{*}(\mathbf{R}_{ib},\mathbf{R}_f,t). \tag{2b}$$

We employ the adiabatic approximation for the canonical density of the entire system. In addition, we invoke the high-temperature approximation for the bath density. In the coordinate representation of the bath degrees of freedom, the latter is given by[8]

$$\rho_{ii}(\mathbf{R}_a,\mathbf{R}_b,\beta)$$

$$=\left(\frac{m}{2\pi\hbar^2\beta}\right)^{d/2}\exp\left\{\frac{-m}{2\hbar^2\beta}(\mathbf{R}_a-\mathbf{R}_b)^2 - \frac{\beta}{2}[V_i(\mathbf{R}_a)+V_i(\mathbf{R}_b)]\right\}, \tag{3a}$$

$$=(2\pi\hbar)^{-d}\exp\left\{-\frac{\beta}{2}[V_i(\mathbf{R}_a)+(V_i\mathbf{R}_b)]\right\}\int d\mathbf{P} \times\exp\left[-\frac{\beta P^2}{2m}+\frac{i}{\hbar}\mathbf{P}\cdot(\mathbf{R}_a-\mathbf{R}_b)\right], \tag{3b}$$

where d is the dimensionality of $\mathbf{R}$, $V_i=E_i^v+V^s$ is the potential energy for the bath motion on the initial adiabatic vibrational surface, and $\mathbf{P}$ is the momentum conjugate to $\mathbf{R}$. For simplicity, the previous equation associates the same mass with all the bath coordinates; the extension to different masses is straightforward.[1] From Eq. (3a), it follows that

$$Q_i=\left(\frac{m}{2\pi\hbar^2\beta}\right)^{d/2}\int d\mathbf{R}\exp[-\beta V_i(\mathbf{R})].$$

A semiclassical surface-hopping expression for the $i\rightarrow f$ matrix element of the nonadiabatic propagator $K_{if}(t)$ has been developed earlier.[2] In the coordinate representation of the bath degrees of freedom, the first-order contribution in the nonadiabatic interaction to this propagator is given by

$$K_{if}^{(1)}(\mathbf{R}_i,\mathbf{R}_f,t)=\int d\mathbf{R}_1\ \sigma_{if}^T A_{if}^T e^{-iS_{if}^T/\hbar} + \int d\mathbf{R}_1\ \sigma_{if}^R A_{if}^R e^{-S_{if}^R/\hbar}. \tag{4}$$

Here, S_{if}^{γ}, where γ stands for T or R, is the classical action for the trajectory that starts at $\mathbf{R}_i$, on potential surface i, hops at $\mathbf{R}_1$ to potential surface f, and continues to $\mathbf{R}_f$, all in time t. Energy is conserved in the hop, and the only component of the momentum that changes due to the hop is the one parallel to the nonadiabatic coupling vector

$$\boldsymbol{\eta}_{if}(\mathbf{R})\equiv\langle f|\nabla^b|i\rangle, \tag{5}$$

where ∇^b is the gradient with respect to bath coordinates. A trajectory is labeled T (transmission) if the quantity $\mathbf{P}\cdot\boldsymbol{\eta}_{if}$ does not change sign in the hop, or R (reflection) if this quantity changes sign at the hopping point. For a particular type of trajectory, the $\mathbf{R}_1$ integration is over all possible hopping points. The quantities σ_{if}^T and σ_{if}^R are transition, or hopping, amplitudes for the T- and R-type hops, respectively, and are given by

$$\sigma_{if}^T=\frac{-(P_{i1\|}+P_{f1\|})}{2P_{f1\|}}\,\bar{\eta}_{if}(\mathbf{R}_1) \tag{6a}$$

and

$$\sigma_{if}^R=\frac{-(P_{i1\|}-P_{f1\|})}{2P_{f1\|}}\,\bar{\eta}_{if}(\mathbf{R}_1). \tag{6b}$$

Here, $P_{i1\|}$ and $P_{f1\|}$ are the components of the momentum at the hopping point on the initial and final potential energy surfaces, respectively, which are parallel to $\boldsymbol{\eta}_{if}(\mathbf{R})$ and are defined to be positive. $\bar{\eta}_{if}$ is the magnitude of $\boldsymbol{\eta}_{if}$ multiplied by the sign of $\mathbf{P}_i\cdot\boldsymbol{\eta}_{if}$, where $\mathbf{P}_i$ is the momentum just before the hop. The prefactors A_{if}^{γ} are given by

$$A_{if}^{\gamma}=\left[(-2\pi i\hbar)^{-d}\frac{P_{f1\|}}{P_{i1\|}}\left|\frac{\partial^2 S_{if}^{\gamma}}{\partial\mathbf{R}_i\partial\mathbf{R}_f}\right|\right]^{1/2}, \tag{7}$$

where the factor $(P_{f1\|}/P_{i1\|})$, which is not present in the familiar adiabatic propagator,[5] compensates for the discontinuity in $\partial^2 S_{if}^{\gamma}/(\partial\mathbf{R}_i\partial\mathbf{R}_f)=\partial P_f/\partial\mathbf{R}_i$ at the hopping point.

The employment of Eq. (4) for the two propagators appearing in Eq. (2b) yields a second-order expression in the nonadiabatic interaction for the transition probability. Figure 1 is a schematic representation of the two trajectories [Figs. 1(a) and 1(b)] corresponding to the two propagators, for particular values of the integration variables. Figure 1(a) indicates the $T-T$ contribution, i.e., when the hop in both trajectories is T type, and Fig. 1(b) indicates the $T-R$ contribution, i.e., when one hop is T type and the other is R type (the horizontal dashed line indicates the total energy of the trajectory, which determines the position of the turning point). In general, of course, there are $R-R$ and $R-T$ contributions as well. It is seen that after the second hopping point $\mathbf{R}_{ib}$, the trajectories are identical. In addition, in order for a particular pair of trajectories to contribute appreciably, the initial points $\mathbf{R}_{ia}$ and $\mathbf{R}_{ib}$ must be close due to the presence of the decaying exponential in the canonical density

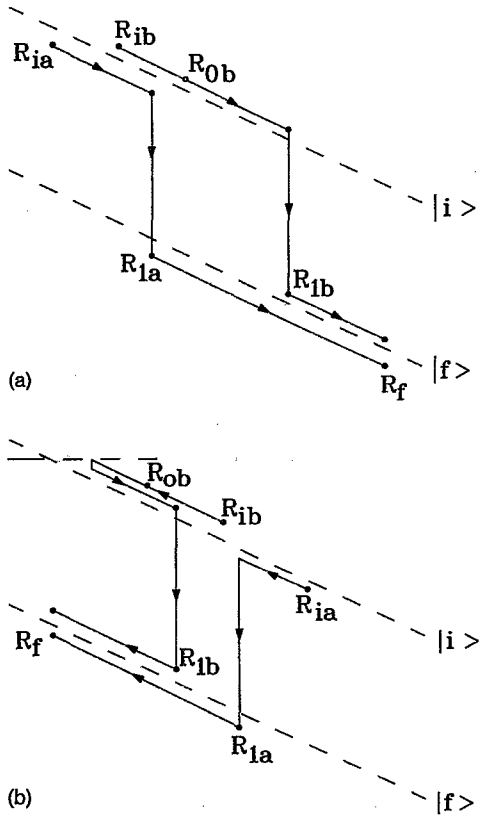

FIG. 1. A schematic representation of the two trajectories corresponding to the two first-order propagators of Eq. (2b). (a) The $T-T$ contribution; (b) the $T-R$ contribution, which, in this case, contains a turning point.

[Eq. (3a)]. This, in turn, implies that the time difference between the two hopping points must be relatively small.

In the next section, results from calculations on a model system with a single bath coordinate are presented. For a one-dimensional bath, after substitution of Eqs. (3b) and (4) into Eq. (2b), the resulting expression can be reduced to the following equation for the second-order transition probability:[1]

$$P_{if}^{(2)}(t)=(\pi\hbar\mu^2 Q_i)^{-1}\,\mathrm{Re}\int dR_{1b}\int dP_{i1b}\int_0^t d\tau(t-\tau)F \times\exp(-\beta E+i\phi/\hbar), \tag{8a}$$

where

$$F\equiv|P_{f1a}|\left|\frac{P_{i1b}P_{f1b}P_{f1a}}{P_{i1a}}\right|^{1/2}\left\{\mathrm{sign}[P_{i1a}\eta_{if}(R_{1a})]\times\frac{(|P_{i1a}|+|P_{f1a}|)}{2|P_{f1a}|}\left|\eta_{if}(\mathbf{R}_{1a})\right|\right\}\times\left\{\mathrm{sign}[P_{i1b}\eta_{if}(\mathbf{R})]\,\frac{(|P_{i1b}|+|P_{f1b}|)}{2|P_{f1b}|}\left|\eta_{if}(\mathbf{R}_{1b})\right|\right\}, \tag{8b}$$

and

$$\phi\equiv\int_0^\tau 2(T_a-T_b)dt-P_{0b}(\mathbf{R}_{0b}-\mathbf{R}_{1a})+(n_b-n_a)\pi\hbar/2. \tag{8c}$$

In Eq. (8a), μ is the mass associated with the coordinate R, τ is the time interval between the hops of the two trajectories, and $E=P_{i1b}^2/(2\mu)+V_i(R_{ib})$ is the total energy of the trajectories. In Eq. (8c), T_a and T_b are the kinetic energies associated with trajectories a and b, (R_{0b},P_{0b}) is the phase-space point of the b trajectory at the time when the a trajectory hops at R_{1a}, and n_a and n_b are the number of turning points of trajectories a and b. In the last two equations, we have indicated only the $T-T$ term. For the $T-R$, $R-R$, and $R-T$ contributions, the + signs appearing in the expressions in curly brackets of Eq. (8b) must be replaced by the combinations $(+,-)$, $(-,-)$ and $(-,+)$, respectively [see Eqs. (6)].

The resulting trajectory corresponding to the integrand of Eq. (8a) runs from R_{1a} to R_{1b} on the lower potential energy surface, and the resulting b trajectory runs from R_{0b} to R_{1b} on the upper surface (see Fig. 1). Hence, it is seen that the only portions of the trajectories that contribute to the integrand are the ones between the hopping points.

Since the time interval between hopping points τ for trajectories that contribute appreciably to the integral of Eq. (8a) is expected to be small, after long enough τ, say $\tau_{\max}$, the integral should change negligibly. If this is the case, then for $t>\tau_{\max}$, we can write

$$P_{if}^{(2)}(t)\to k_{if}t-I, \quad t>\tau_{\max}, \tag{9a}$$

where

$$k_{if}\equiv(\pi\hbar\mu^2 Q_1)^{-1}\,\mathrm{Re}\int dR_{1b}\int dP_{i1b}\int_0^{\tau_{\max}} d\tau\, F \times\exp(-\beta E+i\phi/\hbar), \tag{9b}$$

and

$$I\equiv(\pi\hbar\mu^2 Q_i)^{-1}\,\mathrm{Re}\int dR_{1b}\int dP_{i1b}\int_0^{\tau_{\max}} d\tau\,\tau F \times\exp(-\beta E+i\phi/\hbar). \tag{9c}$$

Hence, the second-order transition probability eventually becomes linear in time, with the slope (i.e., the vibrational-relaxation rate constant) and the intercept given by Eqs. (9b) and (9c), respectively.

It is seen that the relaxation rate constant can be extracted either by measuring the slope of the second-order transition probability in the long-time limit, or by computing the integral of Eq. (9b) directly. Moreover, for sufficiently long time, the relaxation rate constant can also be extracted from

$$P_{if}^{(2)}(t)/t\to k_{if}-I/t, \quad t>\tau_{\max} \tag{10}$$

since the term I/t eventually becomes negligible. The convergence of Eqs. (9) and (10) for finite $\tau_{\max}$ will be numerically investigated in the next section.

It is worth noticing that Eq. (9b) is similar to the one employed in approaches based on the golden rule, in which the rate constant is obtained from the Fourier transform of an appropriate correlation function.[7] This is consistent with the fact that both Eq. (9b) and the golden rule are long-time limit results.

III. RESULTS AND DISCUSSION

In this section, numerical results are reported for a simple one-dimensional model system consisting of a bromine molecule enclosed between two fixed argon atoms. Thus, in Eqs. (8a), (9b), and (9c), μ corresponds to the reduced mass of the diatomic, and R and P correspond to the position and momentum of its center of mass.

In this work, we focus on transitions between the first excited and the ground adiabatic vibrational states. For simplicity, the diatomic molecule is modeled as a harmonic oscillator. The r dependence of the argon–bromine interaction potential, in turn, is approximated by the linear term of its expansion about the equilibrium bond length of the diatomic r_e since the amplitude of the vibrational motion is relatively small. The expressions for the vibrational potential energy curves and the nonadiabatic coupling are taken from Ref. 3. The potential energy function associated with the nth adiabatic vibrational state is given by

$$V_n(R)=V_{\mathrm{int}}(r_e,R)+(n+\tfrac{1}{2})\hbar\omega, \tag{11}$$

where ω is the vibrational frequency of the diatomic. The argon–bromine interaction potential is written as a sum of Lennard-Jones interactions

$$V_{\mathrm{int}}(r,R)=\sum_{k=1}^{2}[V_{\mathrm{LJ}}(R_{Ak})+V_{\mathrm{LJ}}(R_{Bk})], \tag{12}$$

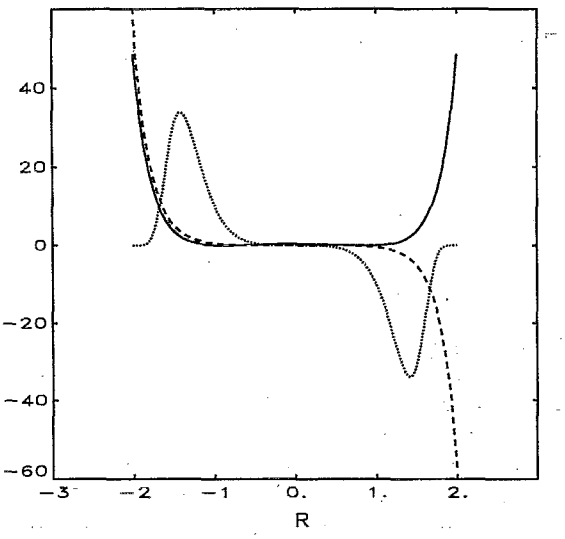

FIG. 2. (Solid line) Model potential [Eq. (11)] multiplied by 0.01 and shifted in energy so that its minimum coincides with zero. (Dashed line) The corresponding nonadiabatic coupling [Eq. (14)]. (Dotted line) The product $\eta_{if}(R)\exp[-\beta V(R)]$ multiplied by 20.0. This figure shows that, in general, the nonadiabatic interaction is effectively localized within narrow regions of the potential.

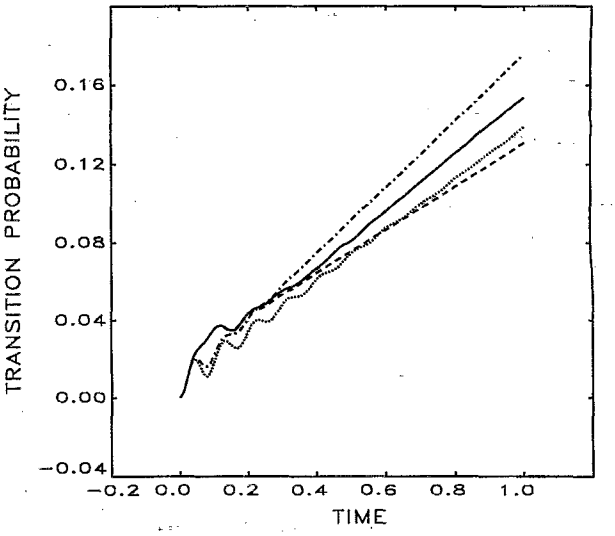

FIG. 3. (Solid line) The second-order transition probability $P_{if}^{(2)}(t)$ [Eq. (8a)] (Dashed line) the same as the solid line, but with one argon atom removed. (Dotted line) the same as the solid line, but employing the local-linear and local-constant approximations for the potential and coupling, respectively. (Dashed–dotted line) the same as the dotted line, but introducing the damping factor $\exp(-\delta\tau)$ in the τ integral.

where, e.g.,

$$V_{\mathrm{LJ}}(R_{Ak})=4\epsilon\left[\left(\frac{\sigma}{R_{Ak}}\right)^{12}-\left(\frac{\sigma}{R_{Ak}}\right)^{6}\right]. \tag{13}$$

In the previous two equations, A and B refer to the two atomic centers in the diatomic and k labels the two argon atoms. The distances R_{Ak} and R_{Bk} are given by $|R_A-R_k|$ and $|R_B-R_k|$, respectively, and R_A and R_B are expressed in terms of the diatomic bond length r and center of mass R as $R_A=R-r/2$ and $R_B=R+r/2$. Notice that the separation between any two potential energy curves in this model is $\Delta V=\hbar\omega$, a constant independent of R. In Eq. (11), a term for the argon–argon interaction potential has not been included since, in this case, it would contribute only a constant. The nonadiabatic coupling $\eta_{if}(R)$ is evaluated as

$$\eta_{if}(R)=\left(\frac{1}{\hbar\mu\omega^{3}}\right)^{1/2}\left[\delta_{i,f-1}\left(\frac{f}{2}\right)^{1/2}-\delta_{i,f+1}\left(\frac{i}{2}\right)^{1/2}\right]\times\left(\frac{\partial^{2}V_{sd}}{\partial r\,\partial R}\right)_{r=r_e}. \tag{14}$$

In this work, reduced units (r.u.) are employed, where time is given in picoseconds, length is given in Angstroms, and energy is given in degrees Kelvin, such that $k_B=1$. It follows that 1 reduced unit of mass (rmu) equals 0.826 amu, and $\hbar=7.65$ K ps. In these units, the potential parameters for Br_2 in Ar are $r_e=2.28$ Å, $\omega=60$ ps^{-1}, $\epsilon=143$ K, and $\sigma=3.51$ Å. The argon atoms were located at -6.0 and $+6.0$ Å. A potential energy curve and its corresponding nonadiabatic coupling are illustrated by the solid and dashed lines of Fig. 2, respectively.

The strategy employed for the efficient numerical evaluation of Eq. (8a) or Eq. (9b) was explained in Ref. 1.

The solid line of Fig. 3 illustrates the calculated second-order transition probability [Eq. (8a)]. It is seen that the expected linear temporal behavior [Eq. (9a)] is attained relatively quickly after a short-time transient regime. The relaxation rate constant, as given by the slope of the linear part of this function, has a value of 0.14 ps^{-1}.

The solid line of Fig. 4 shows the accumulation of the relaxation rate [Eq. (9b)] as a function of the upper limit of the τ integration t converged in R_{1b} and P_{i1b}. It is apparent that, at first, the amplitude of the oscillations decreases rapidly with time. However, after about 0.4 ps, additional oscillations appear. The origins of this structure can be understood as follows:

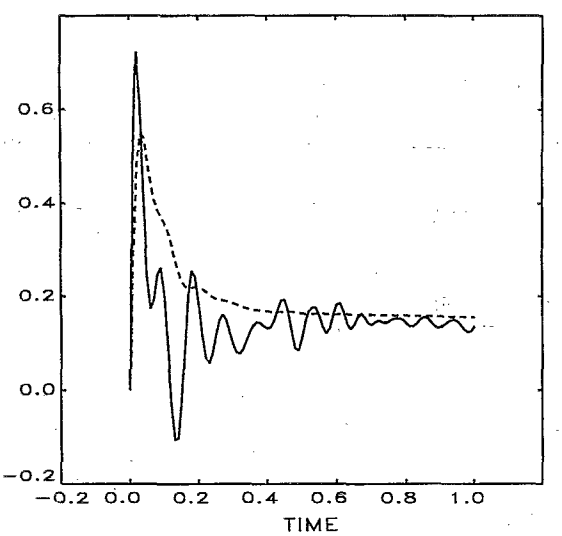

FIG. 4. (Solid line) The accumulation of k_{if} [Eq. (9b)] for the increasing values of the upper limit of the τ integral. (Dashed line) The function $P^{(2)}(t)/t$ [Eq. (10)].

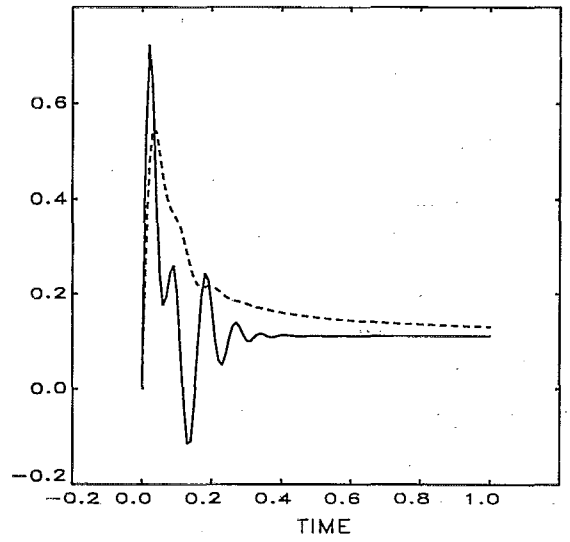

FIG. 5. The same as Fig. 4, except that one of the argon atoms is removed. This figure illustrates the relatively rapid convergence of $P_{if}^{(2)}(t)$ and k_{if} with respect to the upper limit of the τ integral t and explains the origins of the recurrence evident in Fig. 4.

The integrands of Eqs. (8a) and (9b) contain the factors $\eta(R_{1b})$ and $\exp[-\beta V_i(R_{1b})]$, whose product is shown by the dotted line of Fig. 1. It is seen that due to the exponentially decaying weighing factor, the nonadiabatic coupling is effectively localized within small regions of the potential. If a trajectory is run starting at the position of one of the peaks with zero momentum on the initial curve, hopping immediately to the final curve and traveling to the other peak, the time to complete it is found to be about 0.5 ps. Thus, it is apparent that the structure originates from the onset of new contributions to the integral as the center of mass of the diatomic travels from the neighborhood of one argon atom to the other. Indeed, if one of the argon atoms is removed, the structure disappears, as shown by the solid line of Fig. 5. This effect arises in this particular problem because of the confining nature of the one-dimensional model potential. In a realistic, multidimensional problem, the averaging over solvent configurations should wash out this structure due to the phase cancellation between the two solvent trajectories.

Therefore, the τ integrals of Eqs. (8a) and (9b) converge relatively quickly, i.e, $\tau_{\max}$ is relatively small, meaning that only small values of τ contribute to the relaxation rate constant. This can also be illustrated by calculating the second-order transition probability (8a) with one argon atom removed, which is shown by the dashed line of Fig. 3. It is seen that after about 0.4 ps, the plot becomes perfectly linear. (The slope, however, is not the same since the potential has been altered.) The value of the accumulation of the rate constant [Eq. (9b)] at $t=0.4$ ps, when it would converge were it not for the recurrence, is about 0.14 ps^{-1}, in agreement with the value obtained from the solid line of Fig. 3.

The dashed lines of Figs. 4 and 5 represent the function $P_{if}^{(2)}(t)/t$ calculated with the full potential and with one argon atom removed, respectively. Since we have found that $P_{if}^{(2)}(t)$ converges at about $\tau_{\max}=0.4$ ps, the slowly decaying tail remaining after this time must come from the $1/t$ term of Eq. (10). Thus, due to the $1/t$ tail, in a realistic problem, this function should converge to the rate constant more slowly than the function represented by the solid lines [Eq. (9b)]. In fact, from Fig. 4, we obtain that, at $t=1.0$ ps, $P_{if}^{(2)}/t=0.16$ ps^{-1}. It must be kept in mind that the function represented by the solid lines can be interpreted as the relaxation rate constant [Eq. (9b)] only in the long-time limit. Therefore, the short-time oscillations of this function, which cause it to assume negative values at certain times, are of no concern.

The fast convergence of the τ integral suggests that a model based on local approximations for the potential and the nonadiabatic coupling should provide accurate results. By local, it is meant that for a trajectory specified by a particular R_{1b}, certain quantities are evaluated only at this point and assumed to be constant during the rest of the trajectory. The crudest level of approximation is to consider both the potential and the coupling to be locally constant. It can be shown analytically that this approximation predicts a relaxation rate constant equal to zero. Here we study an approximation in which the potential is assumed to be locally linear and the coupling is assumed to be locally constant. Thus, the slope of the potential (i.e., the force) and the coupling are evaluated at R_{1b} and assumed to be the same for the rest of the trajectory. (In a realistic, multidimensional problem, this represents enormous computational savings, since the force needs to be evaluated only once for a particular trajectory.)

The dotted line of Fig. 3 illustrates the second-order transition probability (8a) calculated with the locally linear potential and the locally constant coupling. Evidently this function is shifted to smaller values in comparison with the "exact" calculation (solid line), and very slight oscillations survive in the long-time regime. However, the slopes of the two curves are seen to be nearly the same. Indeed, the slope of the (approximately) linear part of the dashed line is estimated to be 0.13 ps^{-1}, which is close to the previously found exact value of 0.14 ps^{-1}.

The solid line of Fig. 6 shows the accumulation of the rate constant [Eq. (9b)] and the dashed line shows $P_{if}^{(2)}(t)/t$ [Eq. (11)] calculated with this local approximation for the potential and coupling. At $t=1.0$ ps, the latter function assumes the value of 0.13 ps^{-1}. The accumulation of the rate constant (solid line) displays decaying-amplitude oscillations even in the long-time regime. In contrast with Fig. 4, these oscillations are not due to the nature of the model, but to the approximation, since they were found to persist after one of the argon atoms was removed. The solid line in Fig. 6 averaged over the last oscillation is estimated to be about 0.12 ps^{-1}, which is close to the slope of the dotted line of Fig. 3.

After a sufficiently long time, these oscillations should eventually die out. In order to avoid having to carry out the calculation to long time, the factor $\exp(-\delta\tau)$ can be introduced in the integrand of Eqs. (8a) and (9b) in order to further damp the oscillations. The dashed–dotted line of Fig. 3 illustrates the result of such a calculation for the transition probability with $\delta=5.0$ ps^{-1}. Figure 7, in turn, illustrates the result of this calculation for the accumulation of the rate constant (solid line) and $P_{if}^{(2)}(t)/t$ (dashed lined). The solid line converges to 0.17 ps^{-1}, in accordance with the slope of the dotted line of Fig. 3. At $t=1.0$ ps, it is seen that

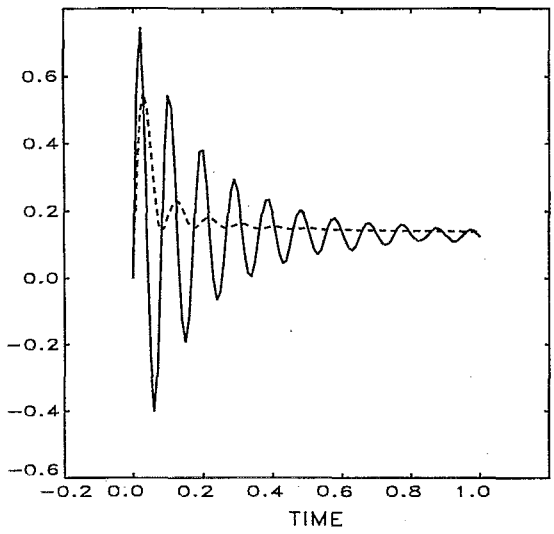

FIG. 6. The same as Fig. 4, except that the local-linear and local-constant approximations for the potential and coupling, respectively, have been employed.

$P_{if}^{(2)}(t)/t=0.18\ \mathrm{ps}^{-1}$. Thus, it is possible to obtain a reasonably good approximation for the rate constant from Eq. (10b) within the local approximation, with a relatively small range of τ, by following this procedure. Naturally, the stronger the damping, the faster the convergence, but at the same time, the poorer the approximation. The choice of δ involves a controlled compromise between the amount of computation time one is willing to spend and the accuracy one wishes to achieve.

In summary, for a multidimensional problem, where recurrences of the type discussed above are not expected to arise, Eqs. (8a) and (9b) provide efficient schemes for the evaluation of the vibrational-relaxation rate constant. This is due to the fast convergence of the τ integral. The scheme implied by Eq. (10) necessitates longer integration times due to the $1/t$ tail. It has also been shown that good accuracy can be obtained with local approximations for the adiabatic vibrational surfaces and the nonadiabatic coupling. However, in this case, convergence requires a little longer times than the exact calculation. If desired, faster convergence, with some sacrifice in accuracy, can be forced upon the calculation by introducing a damping factor in the τ integral. Although employment of the local approximation requires slightly longer integration times, the enormous computational savings represented by having to evaluate the force only once for a particular trajectory more than compensate for this drawback.

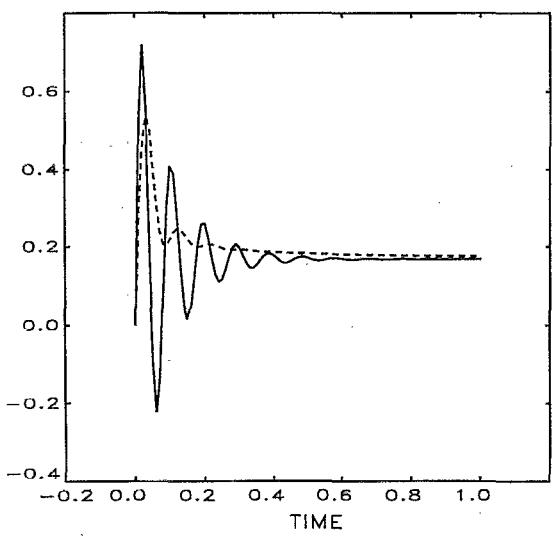

FIG. 7. The same as Fig. 6, but introducing the damping factor $\exp(-\delta\tau)$ in the τ integral.

IV. CONCLUSIONS

We have devised approximations for the calculation of the rate constants of solvent-induced vibrational transitions in a molecule based on a rigorous semiclassical nonadiabatic surface-hopping formalism.[1] Numerical tests were performed on a simple model of a diatomic molecule enclosed between two fixed atoms.

In this framework, the initial state of the system is described by the joint molecule–bath canonical density, projected onto the initial adiabatic vibrational state. The transition probability is evaluated by propagating this density forward in time and then projecting it onto the final adiabatic vibrational state of interest. The transitions are induced by the nonadiabatic coupling between the vibrational and solvent degrees of freedom, and are accounted for in terms of instantaneous hops of the solvent trajectories between the adiabatic vibrational surfaces involved. These hops conserve energy and the only component of momentum that changes is the one along the nonadiabatic coupling vector.[2]

When the nonadiabatic interaction in the propagator is taken into account to first order, the time-dependent transition probability becomes linear in the long-time limit. We presented three different methods for extracting the vibrational-relaxation rate constant in this limit.

The need to look at the long-time limit may seem to render this approach rather computationally demanding. However, theoretical arguments and computational proof were presented that indicate that, in fact, the long-time regime is attained relatively quickly, for practical purposes. This situation is analogous to what occurs in methods directly based on the golden rule,[7] in which the Fourier transform of the relevant time correlation function can be truncated due to the relatively short lifetime of the latter.

Our approach has the advantages that it allows the study of short-time effects in the transition probability and that the nonadiabatic coupling can, in principle, be taken into account up to any order.

Furthermore, since it is formally rigorous, our method can provide guidance for the development of further approximations whose accuracy can be readily assessed. We tested an approximation in which the adiabatic vibrational surfaces and the nonadiabatic coupling are treated as being locally linear and locally constant, respectively. It was found that this approximation yields accurate results and that the level of desired accuracy can be easily controlled. A locally linear approximation for the vibrational surfaces renders a multidi-

mensional problem separable and, consequently, effectively one dimensional. Hence, these local approximations are more generally applicable to realistic systems, where they should represent considerable computational savings. We plan to apply these methods to the study of vibrational relaxation in clusters and liquids.

ACKNOWLEDGMENT

This work was supported by NSF Grant No. CHE-9108500.

[1] M. F. Herman and J. C. Arce, Chem. Phys. **183**, 335 (1994).
[2] M. F. Herman, J. Chem. Phys. (to be published).
[3] (a) M. F. Herman, J. Chem. Phys. **87**, 4779 (1987); (b) **87**, 4794 (1987).
[4] For example, I. N. Levine, *Quantum Chemistry*, 4th ed. (Prentice–Hall, Englewood Cliffs, NJ, 1991).
[5] For example, M. V. Berry and K. E. Mount, Rep. Prog. Phys. **35**, 315 (1972).
[6] (a) J. C. Tully and R. M. Preston, J. Chem. Phys. **55**, 562 (1971); (b) J. C. Tully, *ibid.* **93**, 4740 (1990).
[7] (a) E. J. Heller, J. Chem. Phys. **68**, 2066 (1978); (b) S. Y. Lee and E. J. Heller, *ibid.* **71**, 4777 (1979); (c) E. Neria and A. Nitzan, *ibid.* **99**, 1109 (1993).
[8] R. P. Feynman and A. R. Hibbs, *Quantum Mechanics and Path Integrals* (McGraw–Hill, New York, 1965).